Chapter I: Introduction

1.1 Transition Metal Oxides

Transition metal oxides are probably the most interesting materials exhibiting varieties of crystal structures, interesting physical properties and show wide range of applications. These compounds are composed of oxygen atoms bound to the transition metals. The nature of metal-oxygen bond can change from ionic to covalent depending on the nature of outer d-electrons. The electric properties of these compounds are like insulators (CrO,NiO, CoO,FeO and MnO, $SrTiO_3$), semiconductors (Cu_2O, ZnO, NiO, HfO_2) and conductors (TiO). The diverse magnetic properties of these compounds are diamagnetism (Y_2O_3, TiO_2, CrO_3, AgO), paramagnetism (Ti_2O_3, VO_2), ferromagnetism (CrO_2, $La_{0.5}Sr_{0.5}MnO_3$), ferrimagnetism (Mn_3O_4, γ-Fe_2O_3, $NiFe_2O_4$) and antiferromagnetic (FeO, α-Fe_2O_3, NiO, CoO, Co_3O_4, $LaCrO_3$) at room temperature. These unique properties have applications in tunable microwave device, DRAM cells, infra-red detectors and oxygen sensors. Some complex oxides having perovskite structure like $Pr_{0.7}Ca_{0.3}MnO_3$, $SrZrO_3$, $SrTiO_3$, NiO, TiO_2 and Cu_2O show resistive switching phenomenon which have applications in nonvolatile memories (FeRAM, MRAM, PRAM). The switchable orientation states are possessed by many oxides like $BaTiO_3$, $KNbO_3$ which are ferroelectric and $Gd_2(MoO_4)_3$ which is a ferroelastic material. Transition metal oxides like MoO_3, V_2O_5 and WO_3 have been introduced as sputtering buffer layers of OLED devices. Other transitional metals like TiO_2, ZnO, WO_3 are important for many catalytic process in industries. Among all, few mixed oxides like Fe_3O_4, $MgAl_2O_4$, $FeCr_2O_4$ and $MnFe_2O_4$ exhibits spinel structure with cubic close packing arrangement of atoms.

1.2. Spinels

Among all transition metal oxides, spinels are of general formula AB_2X_4 which crystallizes in cubic crystal system. The anions (X) are typically chalcogens like oxygen and sulfur which are arranged in cubic closed packed structure. The cations may occupy some or all of octahedral and tetrahedral sites in the lattice. While the tetrahedral sites are occupied by divalent (+2) cations and the octahedral sites occupied by the trivalent (+3) cations. When X is occupied by oxygen anion, B site is occupied by Fe, then the spinel is named as ferrites and when B site is occupied by Cr, then th spinel is named as Chromite. Ferrites/chromites are ferrimagnetic in nature. If A site is occupied by non-magnetic elements like Zn, Cd then the compound shows perfect antiferromagnetic behavior.

1.2.1 Structure of spinels

In spinels, AB_2O_4, A is usually a divalent cation such as cobalt (Co^{2+}), Zinc (Zn^{2+}), manganese (Mn^{2+}), nickel (Ni^{2+}), copper (Cu^{2+}), or magnesium (Mg^{2+}) and B is any trivalent cation like Fe^{3+} or Cr^{3+} etc. The oxygen anions (O^{2-}) arrange in a close-packed cubic crystal structure and the cations takes the interstices in two-lattice arrangement. The mineral magnetite (Fe_3O_4) is the first magnetic material discovered in 16^{th} century which is a spinel compound. The minerals are named as spinels after the name of magnesium aluminates ($MgAl_2O_4$).

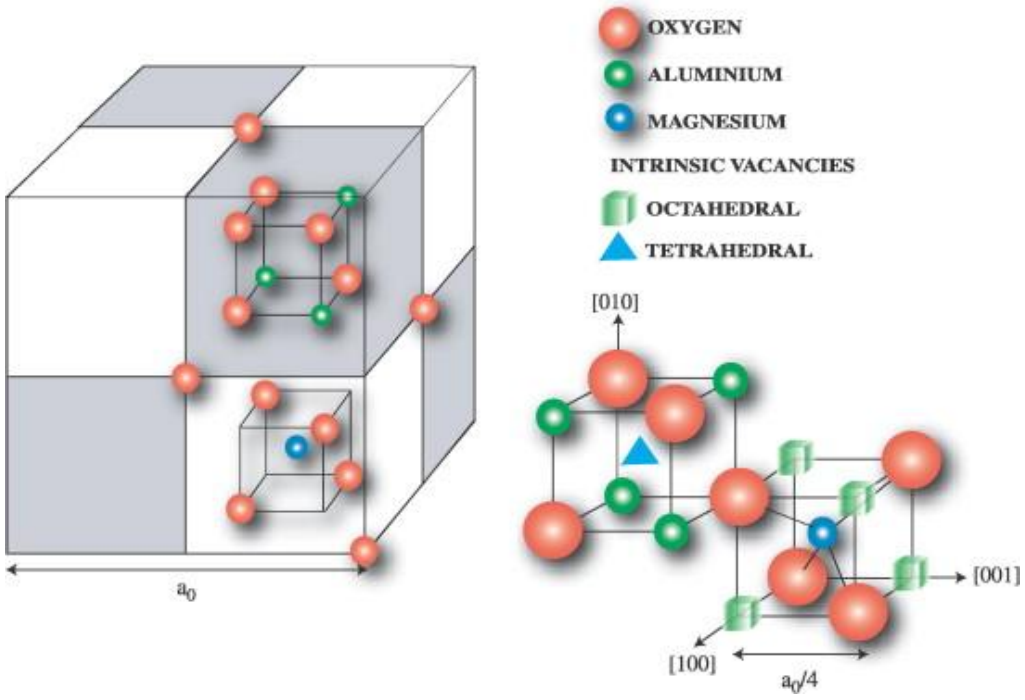

Fig.1.2.1: Crystal structure of spinel $MgAl_2O_4$. [After Sickafus et al. (1999)]

Spinel structure is shown in Fig. 1.2.1. The structure consists of eight formula units,i.e. 8 (AB_2O_4). Total of 8 x7=56 ions are present in a unit cell. While the larger oxygen ions are arranged in FCC structure and the smaller metal ions occupy the interstices. There are two types of voids exits in spinels, a tetrahedral void (A) and the octahedral void (B) as shown in Fig.1.2.2 (a) and (b). Hence the crystallographic environments of the A and B sites are different. Each unit cell consists of 32 oxygen ions in which 8 cations are surrounded by 4 oxygen ions which form tetrahedral sites and 16 cations are coordinated by 6 oxygen ions as octahedral sites. The permanent magnetic moment in spinels arises due to antiparallel alignment and incomplete cancellation of magnetic spins between the A and B. As spinels have cubic structure and no preferred direction of magnetization, it is relatively easy to change the direction of magnetization by external field for which they are called as magnetically soft.

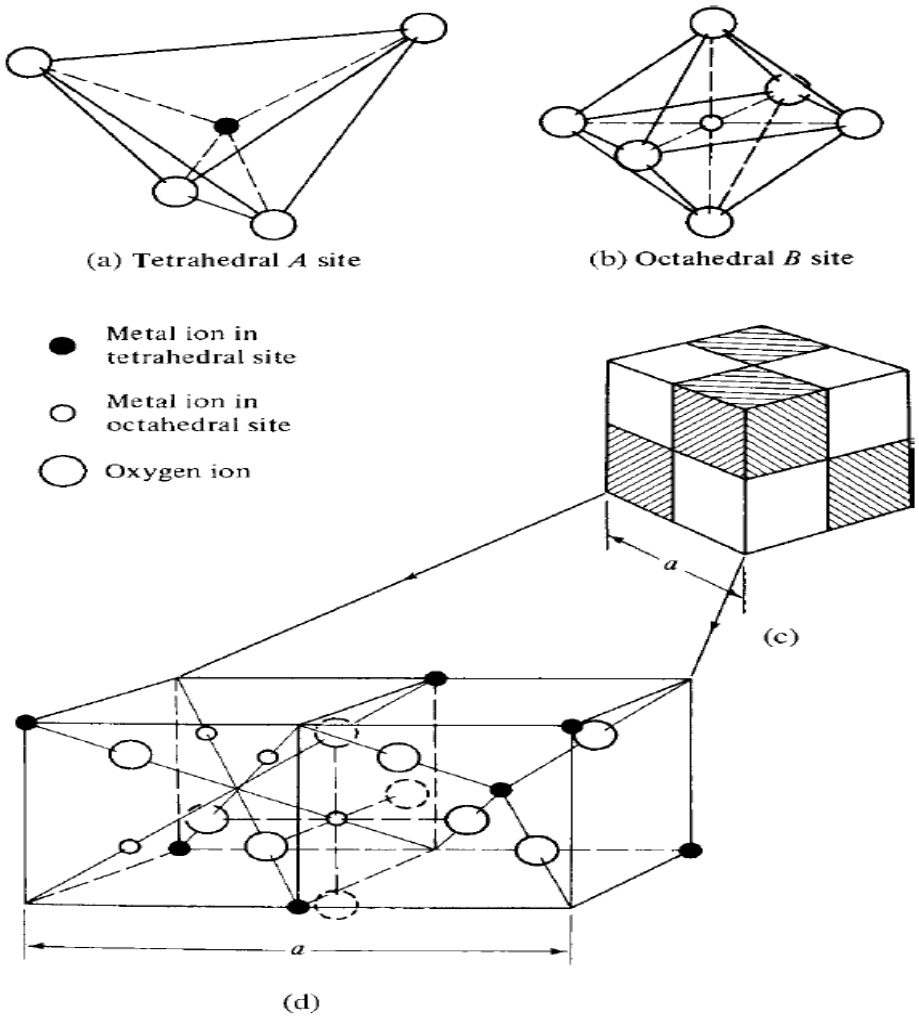

Fig.1.2.2: Crystal structure of cubic spinel and tetrahedral sites and octahedral sites.

[From Cullity et al. (1978)]

The length of unit cell 'a' is divided into eight octants. Now, the length of each edge becomes a/2, as shown in Fig.1.2.2.(c). The four shaded octants are identical with respect to the contents in it, similar to the four unshaded octants. Fig.1.2.2 (d) shows the expanded view of two corner octants. One tetrahedral site can be seen at the center of the right octant of Fig. 1.2.2. (d). There are 4 octahedral sites in the left octant. One is connected by dashed lines to 6 oxygen ions and two are connected by dotted lines are in adjacent octants behind and below. In general, in cubic spinels, all of the available sites

are not occupied by metal ions. Only one-eighth of the A sites and one-half of the B sites are occupied, as shown in Table1.2.2.

1.2.2. Classification of spinles

Based on the cation distribution, spinels are classified into three types.

(a) Normal spinel

(b) Inverse spinel

(c) Mixed spinel

In normal spinel, divalent atoms occupy the tetrahedral site and trivalent atoms occupy the octahedral sites. The normal spinel is represented as: $(D)[T]O_4$ where, the square brackets indicate the octahedral site occupancy, and the parentheses represents tetrahedral sites. D denotes a divalent cation, and T denotes trivalent one. For example, $MgAl_2O_4$ is a normal spinel in which tetrahedral sites are occupied by Mg ions and the octahedral sites are occupied by Al ions. Other few examples of normal spinels are $CoAl_2O_4$, $ZnFe_2O_4$ and $CdFe_2O_4$. In inverse spinel, divalent atoms occupy octahedral site and trivalent atoms occupy both tetrahedral and octahedral sites. Inverse spinel configuration is represented as: $(T)[DT]O_4$. For example, Fe_3O_4 is an inverse spinel in which tetrahedral sites are occupied by Fe^{3+} and octahedral sites are occupied by both Fe^{2+} and Fe^{3+}ions. The other examples of inverse spinel structure are $CoFe_2O_4$ and $NiFe_2O_4$ and $NiAl_2O_4$. Some intermediate structures can also be seen which is called mixed spinel. In mixed spinels, tetrahedral and octahedral sites are occupied by both divalent and trivalent cations. In most of the cases, intermediate cation distribution has been observed, i.e.: $(D_{1-d}\ T_d)[D_d\ T_{2-d}]O_4$

Where, *d* is the inversion parameter or degree of inversion.

d=0, for normal distribution

and d =1, for inverse distribution

In many cases, the degree of inversion depends on the preparation technique, especially on the cooling rate after sintering. The classification of spinles, their structure and examples are given in Table 1.2.1.

Table 1.2.1: Classification of spinels with examples, show the chemical formula and site preference.

Structure of spinel	**Chemical formula**	**Site**		**Examples**
		Tetrahedral	**Octahedral**	
Normal	$(A^{2+})[B^{3+}]\ O^{2-}_4$	A^{2+} cations	B^{3+} cations	$ZnFe_2O_4$ $CdFe_2O_4$ $MgAl_2O_4$
Inverse	$(B^{3+})[A^{2+}B^{3+}]\ O^{2-}_4$	Half of B^{3+} cations	Half of B^{3+} and all A^{2+} cations	$CoFe_2O_4$ Fe_3O_4
Mixed	$(A_{1-d}{}^{2+}B_d{}^{3+})[A_{d/2}{}^{2+}B_{1-d/2}]\ O^{2-}_4$	$0\leq d\leq 1$; d is called as inversion parameter Normal spinel d=0 Inverse spinel d=1		$Ni_xZn_{1-x}Fe_2O_4$ $Mg_xZn_{1-x}Fe_2O_4$

Table 1.2.2: Number of available and number of occupied sites in cubic unit cell of a $MO.Fe_2O_3$ (Where M is the metal ion and O is the oxygen)

site	**Number available**	**Number occupied**	**Spinel**
Tetrahedral (A)	64	8	8 A
Octrahedral (B)	32	16	16 B

If both A and B site is occupied by magnetic ions then the coupling between B site is quite strong which is associated with super-exchange phenomena.

1.2.3. Exchange interaction

In order to understand the magnetic properties in spinel, it is necessary to know the various interactions observed between A and B sites. These interactions can be well explained using Heisenberg's exchange integral.

In general, let us consider two atoms ‘a’ and ‘b’ with one electron each. The total energy can be expressed as:

$$E = \mathrm{Ea} + E_b + Q \pm J_{ex}$$

Where, E_a and E_b are the electron energies of different atoms a and b respectively. Q is the electrostatic (coulomb) interaction energy and J_{ex} is referred as the exchange energy or the exchange integral. J_{ex} arises from the possibility of exchange between electrons, when electron a moves around nucleus b and electron b orbits nucleus a. Except for their spins, both are indistinguishable. Heisenberg showed that, exchange energy can be represented by the relation:

$$E_{ex} = -2JexS_1.S_2 = -2J_{ex}S_1\,S_2\cos\theta$$

Where, E_{ex} is the exchange energy dependent on the relative orientation of one pair of nearest neighbor spins, S_1 and S_2, and ϴ is the relative angle between them. For $J_{ex} > 0$ it show ferromagnetic order which results in minimum energy; for $J_{ex} < 0$, an antiparallel spin arrangement is favoured. For a solid, a summation over all spin pairs is necessary to calculate the total exchange energy. The above interaction is direct exchange type. In spinels, cations are separated by O^{2-} so the exchange interaction is indirect. This indirect exchange is referred as super-exchange interaction.

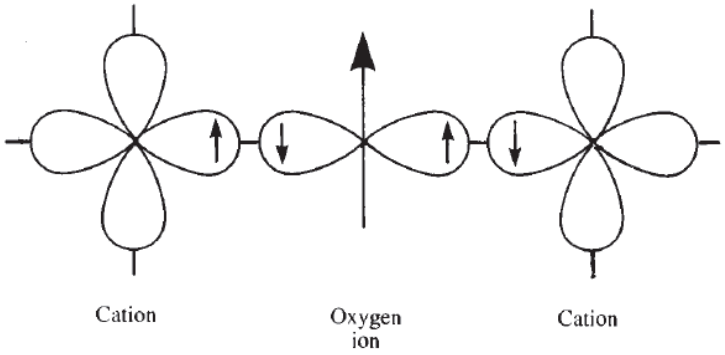

Fig 1.2.3: Schematic representation of super-exchange interaction in magnetic oxides. The p-orbital of anion interact with d orbital of transition metal cations.

Consider two transition metal cations separated by an oxygen ion as shown in Fig. 1.2.3. The O^{2-} has no net magnetic moment since it has completely filled shells, with p-type outermost orbitals. Orbital p_x has two electrons: one with spin up, and the other with spin down, consistent with Pauli's principle. When one of the transition-metal cations is brought close to the O^{2-}, partial electron overlap (between a 3d electron from the cation and a 2p electron from the O^{2-}) can occur only for antiparallel spins, because electrons with the same spin are repelled. Empty 3d states in the cation are available for partial occupation by the O^{2-} electron, with an antiparallel orientation. Electron overlap between

the other cation and the O^{2-} then occurs resulting in antiparallel spins and therefore antiparallel order between the cations. Since p orbitals are linear, the strongest interaction is expected to take place for cation-O^{2-}-cation angles close to 180°.

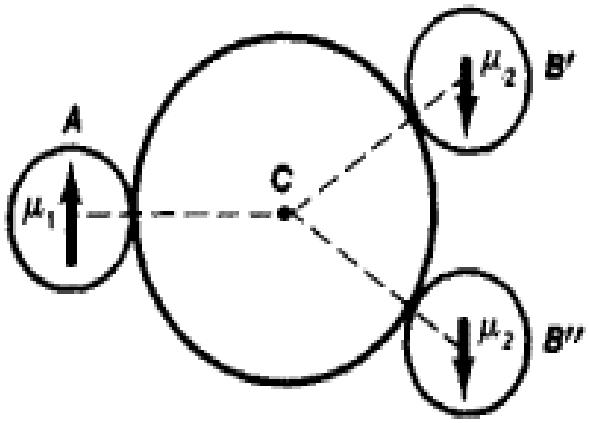

Fig.1.2.4: Schematic diagram representing super-exchange interaction between metal cations A B′ and AB′′ mediated through oxygen ion c.

The strength of anti-parallel coupling between A and B depends on the bond angle A-O-B as shown in Fig. 1.2.4. In collinear ferrimagnetic structure of spinels, A-O-B and B-O-B bong angles are 125°C and 90°C respectively. The distance and angle between cations decides the strength of interaction and hence the magnetic properties. The bond length is inversely proportional while bond angle is directly proportional to the strength of magnetic interaction (A-O-B, B-O-B, A-O-A) [Smit et al. (2017)].

1.2.4. Ferrimagnetism

Spinels exhibits permanent magnetization and show ferrimagnetic behavior. The macroscopic behavior is similar to that of ferromagnets. But the spontaneous magnetization may be quite different due to difference in their internal structure and their temperature effects. In ferrimagnetic materials, the net magnetic moment is non zero as

the magnetic moment of the two sublattice are uncompensated. Such an uncompensated anti-ferromagnetism leads to ferrimagnetism.

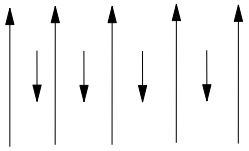

Fig. 1.2.5: The spin orientation of magnetic moments in sub-lattices of a ferrimagnetic material.

Ferrimagnetic materials exhibit spontaneous magnetization below the ferrimagnetic Curie temperature (T_C). The spins are aligned antiparallel to each other but do not cancel out. Hence the net magnetization arises from the antiparallel alignment of spins as shown in Fig 1.2.5. Ferrimagnetic materials exhibit magnetic saturation and hysteresis because of the presence of self-saturated domains. Hence, the susceptibility is very large and positive. Above Curie temperature, the ferrimagnetic material becomes paramagnetic.

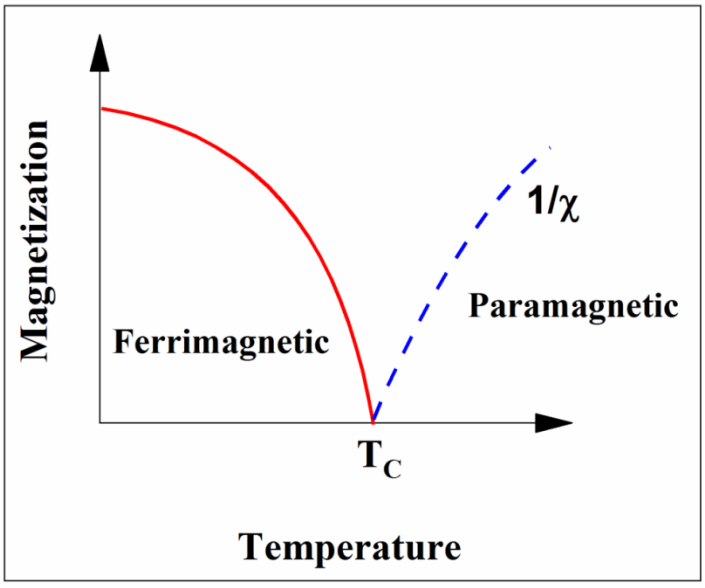

Fig.1.2.6: Temperature dependence of magnetization and susceptibility in ferrimagnetic spinel.

The variation of magnetization and inverse susceptibility with respect to temperature of a ferrimagnetic material is shown in Fig. 1.2.6. The ferrimagnetism and its temperature dependence are well explained using molecular field theory.

Molecular field theory

Molecular field theory is adoptable for ferrimagnetic materials because the magnetic moments are considered to be localized at particular ions. The super-exchange interaction causes the exchange forces between metal ions through oxygen ions. The molecular field theory for ferrimagnetic materials is complicated because even same ions on A and B sites has different arrangement of atoms and different nearest neighbors. Hence, AA interaction will differ from the BB interaction even though the same ions are present at A and B sites.

For example, consider $MO.Fe_2O_3$, to understand the interactions between A and B sites, which has an inverse spinel structure.

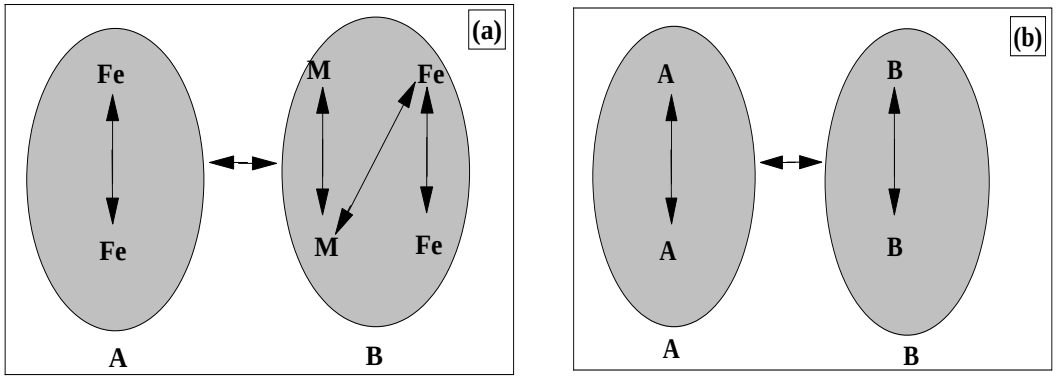

Fig. 1.2.7: (a) Exchange interactions between ions in an cubic inverse ferrite. (b) Modified interactions

When compared with only two antiferromagnetic interactions (A-B and AA; BB), there are five interactions, i.e. one A-A, three B-B and one A-B interactions as shown by arrows in Fig.1.2.7(a). Neel simplified it by considering a model composed of identical magnetic ions which are divided unequally between the A and B sublattices. The interactions are now reduced to two as shown in Fig.1.2.7 (b).

Neel's theory

Let us consider n identical magnetic ions per unit volume in which a fraction of λ ions are located in A sites and a fraction ν (=1- λ) in B sites. At a temperature T, let μ_A be the average moment of A ions in the direction of the field. Then the magnetization of the A sub lattice is $M_A= \lambda n\mu_A$ and the total magnetism is $M= M_A+M_B= \lambda M_a + nM_b$

The molecular field on A sublattice is

$H_{mA}= - \gamma_{AB}M_B + \gamma_{AA} M_A$

Where, the molecular field coefficients γ are taken as positive quantities. While the negative sign denotes the antiparallel interaction between A, B ions and a positive sign for parallel interaction between A ions.

Similarly, $H_{mB}= - \gamma_{AB}M_A + \gamma_{BB} M_B$

The coefficients γ_{AA} and γ_{BB} are unequal and we express them as $\alpha= \frac{\gamma_{AA}}{\gamma_{AB}}$ and $\beta= \frac{\gamma_{BB}}{\gamma_{AB}}$.

The molecular fields are obtained as

$H_{mA}= \gamma_{AB} (\alpha\lambda M_a-\nu M_b)$

$H_{mB}= \gamma_{AB} (\beta\nu M_b-\lambda M_a)$

These equations are valid above and below the Curie temperature.

Above Curie temperature

In the paramagnetic region, i.e. above curie temperature the Curie-law for each sublattice is expressed as $MT=\rho CH_t$. Where, ρ is the density, H_t is the sum of the applied and molecular field.

After tedious algebra, the expression for mass susceptibility is written as

$$\chi = \frac{M}{\rho H} = \frac{CT - \gamma AB\rho c^2 \lambda\nu(2+\alpha+\beta)}{T^2 - \nu_{AB}\rho CT(\alpha\lambda+\beta\nu)+\rho^2 C^2 \nu_{AB}{}^2 \lambda\nu(\alpha\beta-1)}$$

It may be written in the form:

$$\frac{1}{\chi} = \frac{T}{C} + \frac{1}{\chi_o} - \frac{b}{T-\Theta}$$

$$\frac{1}{\chi} = \frac{T+\frac{C}{\chi 0}}{C} - \frac{b}{T-\Theta}$$

The plot of above equation 1.1 is shown in Fig. 1.2.8., which represents a hyperbola.

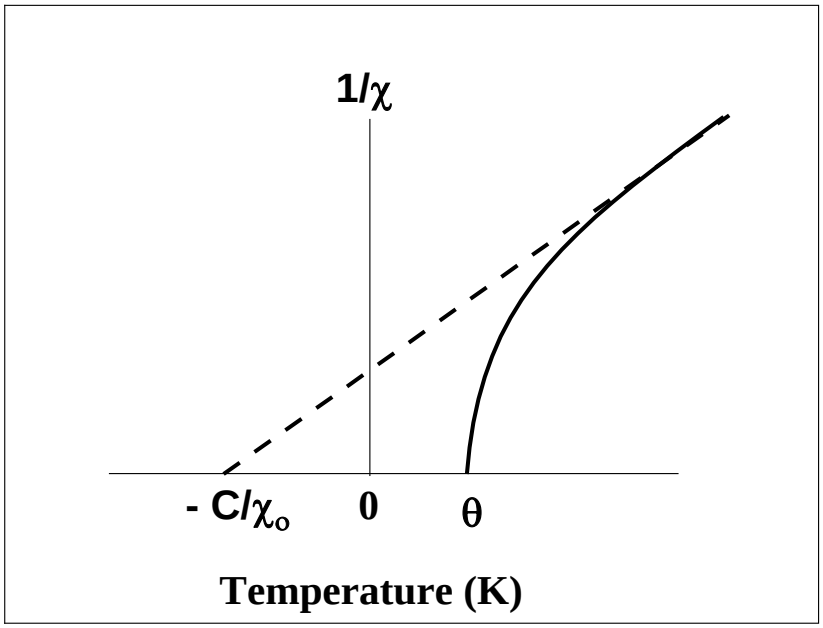

Fig. 1.2.8: Temperature dependence of reciprocal susceptibility above Curie temperature.

It cuts the temperature axis at paramagnetic Curie point (θ). At the high temperature the last term of equation 1.1 is negligible and is reduces to Curie-Weiss law: $\chi = \frac{C}{T+(\frac{C}{\chi o})}$. It is shown in the Fig. 1.2.8 as dashed line which becomes asymptotic at high temperatures.

Below Curie temperature

The molecular field magnetizes each sublattice in ferrimagnetic region. But the net magnetization in two sublattice are opposite to each other. The net magnetization is expressed as

$|M|=|M_A|-|M_B|$.

The ferrimagnetic crystal consists of two magnetic sublattices. The existence of different sublattices in ferrimagnet leads to a complex temperature dependence of spontaneous magnetization.

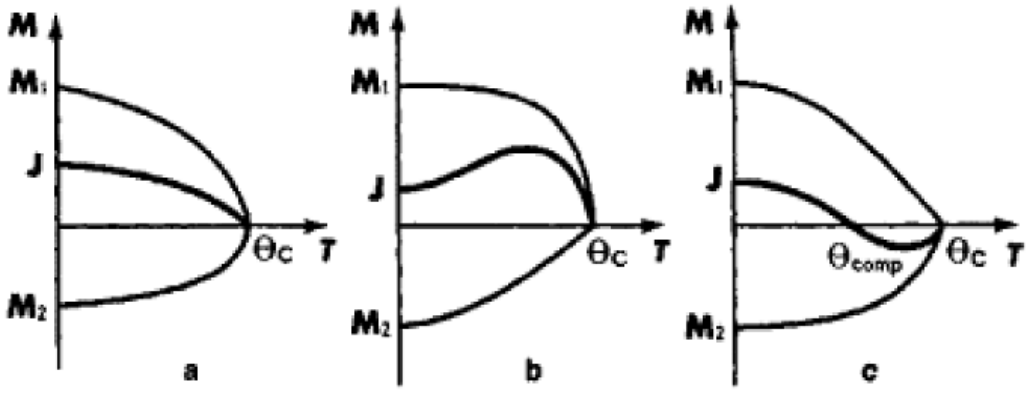

Fig.1.2.9: Different types of temperature dependence of the sub-lattice magnetizations M_1 and M_2 and the spontaneous magnetization J. Here θ_C is the Curie temperature.

Such temperature dependence occurs because the temperature dependences of the magnetization of each sublattice may differ as shown in Fig. 1.2.9. As a result, as temperature increases from absolute zero, the spontaneous magnetization, which is the difference between the sublalttice mangnetization may have three possibilities:

i. decrease monotonically as in ordinary ferromagnet,

ii. increase at low temperature and thereafter pass through some maximum

iii. tend to zero at some specified temperature Θ_{comp}, which is called as compensation point. At $T > \Theta_{comp}$ or $T < \Theta_{comp}$, the spontaneous magnetization is nonzero.

Ferrimagnetis have peculiar magnetic properties near the compensation point, where even weak magnetic fields cause the sublattices to slope and flip relative to each other. Far from the compensation point, such changes in magnetic structure occur in strong magnetic fields i.e. magnetic fields of the same order as the exchange fields. Under certain conditions, resonance absorption of electromagnetic energy is observed in ferrimagnets, such absorption is called ferrimagnetic resonance.

1.2.5 Cationic distribution based on crystal field theory:

The type of cations and their distribution affects the physical properties of spinels like magnetization, anisotropy, magnetostriction and bond length etc. Various factors affect the distribution of cations in the spinels and contribute to the total lattice energy of the spinel. The following factors which affect the cation distribution are:

(a) Elastic energy

(b) Electrostatic energy

(c) Crystal field stabilization energy

(d) Polarization effect

In the elastic and electrostatic energy calculations, the ions are considered as spherically symmetric with only coulombic interaction. However for transitional metal

cations this is different. Hence, the crystal field theory could be applicable to understand the cation distribution of spinels. Crystal field theory (CFT) is used to describe the breaking of degeneracies of electronic orbital states. It occurs due to the static electric field produced by a neighboring anion charge distribution. The charge density of d orbitals which interacts with the charge distribution at which the transition ion is placed is shown in Fig.1.2.10.

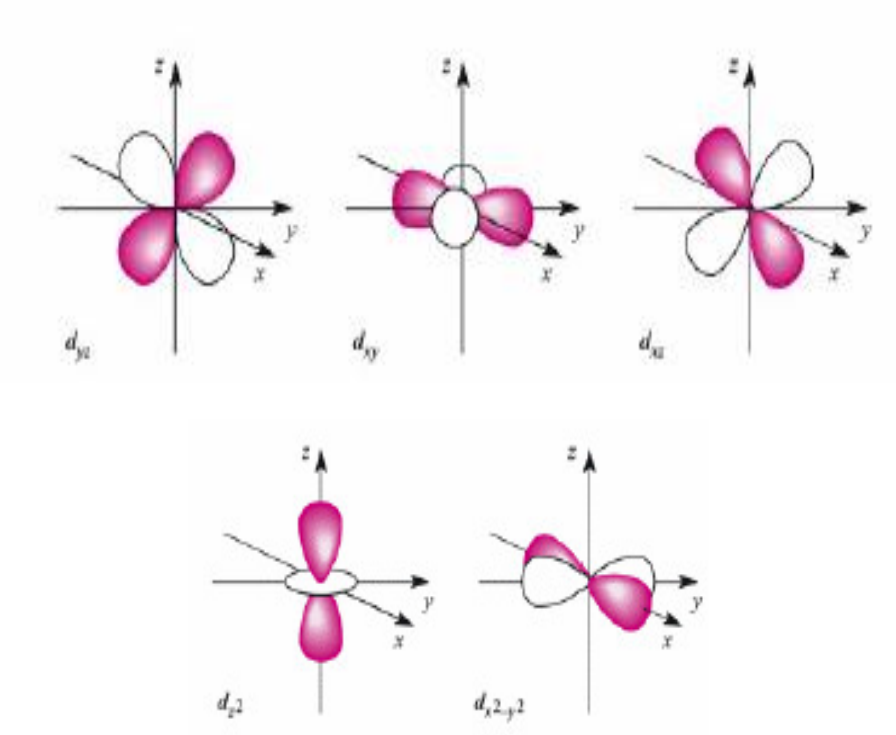

Fig. 1.2.10: Spatial geometry of d-orbitals and their interaction.

The five d orbitals (commonly designated as d_{xy}, d_{yz}, d_{zx}, d_z^2 and $d_{x^2-y^2}$) split based on the symmetry of the electrostatic field produced by particular lattice site anions. The splitting

is due to the electrostatic repulsion between the d electrons and the electrons of surrounding anions.

In an octahedral field, the energy level splits in to two orbital groups. A lower triplet formed by d_{xy}, d_{yz} and d_{zx} orbitals and a higher doublet with d_z^2 and $d_{x^2-y^2}$ orbitals. When these orbitals point directly to the anions then the the energy of the doublet increases. The energy of the triplet decreases when the orbitals direct to regions of low electron density. Δ denotes the energy difference between the triplet (t_{2g}) and the doublet (e_g) states.

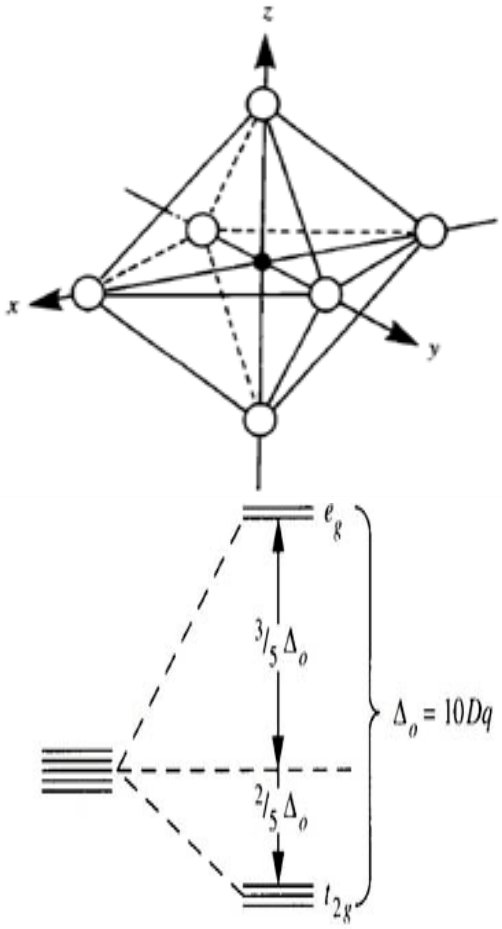

Fig 1.2.11: The metal cation in octahedral field and its energy level diagram.

The splitting is reversed in case of tetrahedral sites and the energy of doublet is lower than energy of triplet. The energy difference in terms of tetrahedrally coordinated cations is 4/9 times that of the octahedral coordination.

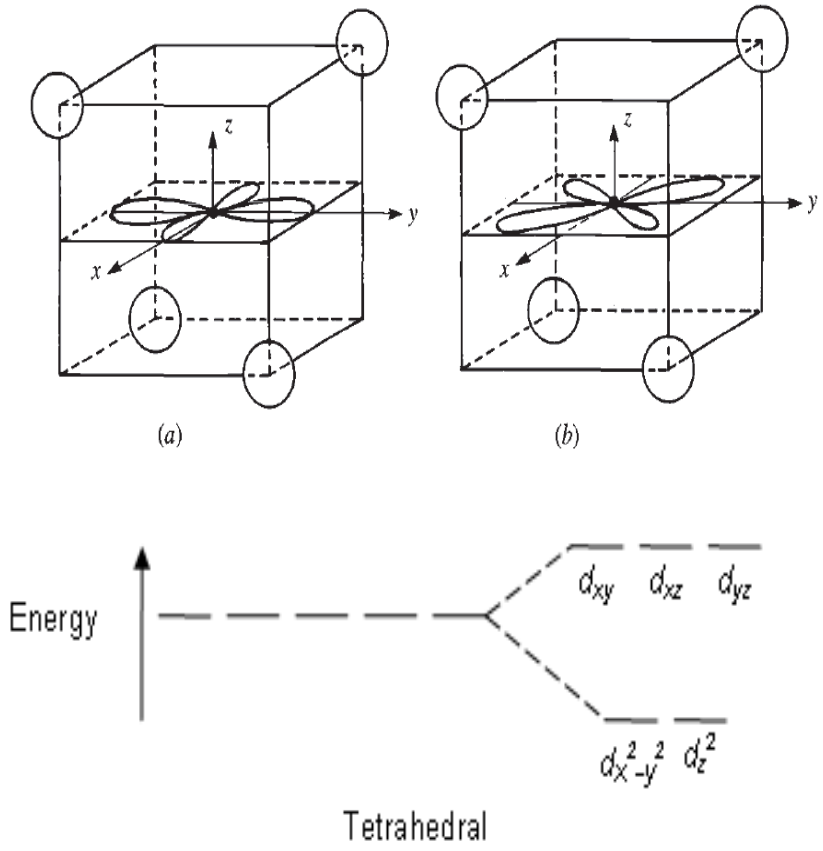

Fig. 1.2.12: Transition-metal cation in a tetrahedral coordination; *(a)* d_{x2-y2} orbital, *(b)* d_{xy} orbital (c) corresponding schematic energy level diagram.

The energy t_{2g} is stabilized by amount -0.4 Δ and e_g level is destabilized by + 0.6 Δ (+ve sign increase in energy, -ve sign decrease in energy). Splitting Δ depends on the following factors:

•Nature of the ligands

•The charge on the metal ion

• Metal belongs to 3d, 4d, or 5d element

By considering the above factors, the crystal field stabilization energies (CFSE) for d^0 to d^{10} configurations and the Octahedral Site Preference Energies (OSPE) are calculated as follows:

$$OSPE = CFSE\ (oct) - CFSE\ (tet)$$

$$\text{where,} \quad \Delta_{tet} = \Delta_{oct} * 4/9$$

The following table gives the calculated CFSE and OSPE values of d- electrons.

Table1.2.3: CFSE and OSPE energies of d-electrons.

Crystal Field Stabilisation Energies (CFSE) and Octahedral Site Preference Energies (OSPE)					
d-electrons	**Octahedral**		**Tetrahedral**		**OSPE**
		CFSE		**CFSE**	
d^0	t_{2g}^0	0 Δo	e^0	0 Δt	0 Δo
d^1	t_{2g}^1	-2/5 Δo	e^1	-3/5 Δt	-6/45 Δo
d^2	t_{2g}^2	-4/5 Δo	e^2	-6/5 Δt	-12/45 Δo
d^3	t_{2g}^3	-6/5 Δo	$e^2t_2^1$	-4/5 Δt	-38/45 Δo
d^4	$t_{2g}^3e_g^1$	-3/5 Δo	$e^2t_2^2$	-2/5 Δt	-19/45 Δo
d^5	$t_{2g}^3e_g^2$	0 Δo	$e^2t_2^3$	0 Δt	0 Δo
d^6	$t_{2g}^4e_g^2$	-2/5 Δo + P	$e^3t_2^3$	-3/5 Δt + P	-6/45 Δo
d^7	$t_{2g}^5e_g^2$	-4/5 Δo + 2P	$e^4t_2^3$	-6/5 Δt + 2P	-12/45 Δo
d^8	$t_{2g}^6e_g^2$	-6/5 Δo + 3P	$e^4t_2^4$	-4/5 Δt + 3P	-38/45 Δo
d^9	$t_{2g}^6e_g^3$	-3/5 Δo + 4P	$e^4t_2^5$	-2/5 Δt + 4P	-19/45 Δo
d^{10}	$t_{2g}^6e_g^4$	0 Δo	$e^4t_2^6$	0 Δt	0 Δo

Particularly, one can estimate the CFSE for octahedral site in eV and are shown in Table 1.2.4.

Table 1.2.4: Estimated OSPE of various cations with No. of d electrons.

No. of d electrons	Cations	Estimated OSPE (eV)
1	Ti^{3+}	0.33
2	V^{3+}	0.53
3	V^{2+} Cr^{3+}	1.37 2.02
4	Mn^{3+} Cr^{2+}	1.10 0.74
5	Fe^{3+} Mn^{2+}	0 0
6	Fe^{2+} Co^{3+}	0.17 0.82
7	Co^{2+}	0.09
8	Ni^{2+}	0.99
9	Cu^{2+}	0.68
10	Zn^{2+}	0

The above table gives the information about the site occupancy of cation in A and B sites. From Table 1.2.4, it is observed that among all transition metal ions, Cr^{3+} has highest octahedral site preferential energy and Fe^{3+} has least energy, i.e. zero. Hence, Cr^{3+} ions

always occupy B site irrespective of A site cation. In particular, $NiCr_2O_4$, $CoCr_2O_4$ are normal spinels where as $NiFe_2O_4$ and $CoFe_2O_4$ are inverse spinels. Being Cr in B site, B-B interaction in chromites is stronger than A-B interaction. Hence, chromites show unusual magnetic ordering which are not observed in ferrites.

1.3. Chromites

Chromites are spinel compounds with general formula ACr_2O_4. They have normal spinel structure in which A-site is occupied by divalent cation (Mn^{2+}, Ni^{2+}, Co^{2+}, Zn^{2+}, Cu^{2+}, or Mg^{2+}) and B-site is occupied by trivalent cation (Cr^{3+}). The ideal structure is formed by a cubic close-packed FCC array of O atoms. One common chromite is Cobalt Chromite which is a normal spinel. Co^{2+} ionsoccupy tetrahedral site and Cr^{3+} ions occupy octahedral sites because Cr^{3+} ions have the strong octahedral site preferential energy (2.02 eV). In $CoFe_2O_4$, as Fe is having less octahedral site preferential energy, $CoFe_2O_4$ is having inverse spinel structure. $CoCr_2O_4$ crystallizes in a cubic Fd-3m structure. In the crystal field of O^{2-} ions, the $3d^3$ orbits of Cr^{3+} ions split into two. One is a half-filled t_{2g} triplet with lower energy and other is an empty e_g doublet with higher energy. While, the $3d^7$ orbits of Co^{2+} split into full-filled e_g doublet having the lower energy and half-filled t_2 triplet with higher energy. In $CoCr_2O_4$, both Co^{2+} and Cr^{3+} are being magnetic ions, a complex phase diagram is observed when compared with ACr_2O_4, where A is a non-magnetic ion. This could be due to the presence of magnetic moment and orbital degeneracy on the A-site ions. Because of strong competing interaction between J_{AB} and J_{BB}, the magnetic ground state of $CoCr_2O_4$ is stable. Hence, the system displays typical helical ordering and a complex sequence of magnetic transitions.

1.4. Applications of chromites

Chromites have enormous applications in industry. For example, Nickel chromite ($NiCr_2O_4$) is commonly used as catalytic material [Jebarathinam et al. 1994], gas sensors [Honeybourne et al. 1996] and as high-temperature oxidation products of Ni-containing alloys [Strawbridge 1993]. $CoCr_2O_4$ is an electronically conductive oxide stable in air which is a potential material for application as material to interconnect cells of a high-temperature zirconia-electrolyte in fuel-cell battery [Sun et al. 1972]. Multiferroic nature has been observed in various chromites by mixing A and B site cations with either magnetic or non magnetic ions. $CoCr_2O_4$ is spinel where the spiral component induces an electric polarization for which it is called as multiferroic material [Yamasaki et al. 2006]. In addition, Cobalt chromite is used as catalyst for combustion of chlorinated organic pollutants [Kim et al. 2001] and catalyst for methane combustion [Hu et al. 2014]. $ZnCr_2O_4$-K_2CrO_4 ionic conductive ceramic sensor is used as humidity sensor [Bayhan et al. 2006]. $CuCr_2O_4$ is a versatile catalyst which is used in production of clean energy, drugs and agro chemicals etc. Nickel/copper chromite catalysts are used for hydrogenating edible oils [Moulton et al. 1974]. An extruded copper chromite-alumina catalyst is prepared by blending together from 40-82 % by weight of copper chromite and 18-60% of an extrudable alumina. This is used as hydrogenation catalyst. Zinc iron chromite is used as pigments [Murdock et al. 1988]. It is expected that by changing the composition of chromites, i.e., by substituting magnetic or nonmagnetic ions, one may expand the applications of chromites in multifunctional devices.